Mechanical and magnetic properties of spark plasma sintered soft magnetic FeCo alloy reinforced by carbon nanotubes

Amar J Albaaji[1*], Elinor G Castle[2,3], Mike J Reece[2,3], Jeremy P Hall[1], Sam L Evans[4]

1-Wolfson Centre for Magnetics, Cardiff School of Engineering, Cardiff University, UK

2-School of Engineering and Materials Science, Queen Mary University of London, UK

3-Nanoforce Technology Ltd., London, UK

4-Institute of Mechanical and Manufacturing Engineering, Cardiff School of Engineering, Cardiff University, UK

*Corresponding author at: Wolfson Centre for Magnetics, Cardiff School of Engineering, The Parade, Cardiff University, Cardiff CF24 3AA,UK.

Tel.+44(0)7440731570; Fax:+44 02920874716; E-mail address: amar.jabar@yahoo.com

Keywords: Carbon nanotubes, Spark plasma sintering, soft magnetic

Abstract

Different volume fractions (0.5 vol. % to 4.5 vol. %) of CNTs were used to reinforce a binary Fe50Co soft magnetic alloy. The first method for dispersion was involved dry mixing and ball milling of the powder, while the second was included wet mixing in dimethylformamide under ultrasonic agitation, drying and then dry ball milling. The powders were consolidated using spark plasma sintering. Tensile test and SEM analyses were performed to characterize the mechanical properties and the fracture surface of the sintered materials. The best magnetic and mechanical properties were achieved using the first method. A maximum enhancement in tensile strength of around 20% was observed in the 0.5 vol. % CNT composite with improved elongation compared to the monolithic Fe50Co alloy. In addition, the magnetic properties were enhanced by adding CNTs up to 1 vol. %, and an improvement in densification was observed in composites up to 1.5 vol. % CNT with respect to monolithic Fe50Co alloy.

1. Introduction

It is well known that intermetallic compounds have good soft magnetic properties. FeCo alloys based on intermetallic compounds exhibit high saturation magnetisation (2.45T) and high Curie temperatures (920 - 985 ˚C). In particular, the equiatomic composition exhibits the highest permeability and zero magnetocrystalline anisotropy [1]. However, the ordered Fe50Co alloy is extremely brittle and its' workability is therefore typically improved

by the addition of alloying elements such as 2%wt. vanadium; as in Permendur or FeCo-2V alloy [2]. Such alloying elements lead to the formation of precipitates; improving the mechanical properties yet leading to a deterioration of the magnetic properties. The coercivity in particular is affected by the presence of microstructural defects, such as grain boundaries and dislocations [3]. Equiatomic- iron cobalt alloy is primarily used in applications where the reduction of weight or volume of material is of primary importance [2]. As a result there is a continuous interest in improving the properties of these alloys. The disordered state of this alloy exhibits higher yield strength than the ordered state combined with a change in fracture mode from intergranular to transgranular cleavage [4, 5]. Zhao et al. [6] investigated the effect of constitutional and thermal disorder on the ductility of ordered and disordered FeCo alloys; and concluded from the practical results that the partial disorder at grain boundaries is required to achieve some ductility if an ordered FeCo alloy. Since a dispersion of nanosize reinforcement in FeCo alloy may lead to partial disorder at the grain boundaries, an improvement in ductility may therefore be expected.

Bowen et al. [7] have shown that the mechanical properties, tensile strength and ductility of composite materials are strongly affected by the size of the reinforcement, with tensile strength increasing with reduction in reinforcement size. This strategy for improving mechanical properties can be broadly applied to many light weight alloys. However, there have only been a limited number of studies of iron cobalt alloys with the addition of very fine reinforcement. Composite materials have advantages in comparison to their base alloys, such as a superior creep resistance, and the final properties of the material can be tailored through appropriate selection of the type and volume fraction of reinforcement [8]. The effects of nano-scale reinforcements on the tensile properties of FeCo alloys have not previously been reported.

Carbon nanotubes possess outstanding properties such as an average Young's modulus of 1.8 TPa. This combined with their high aspect ratio with lengths of 1.17 to 5.1μm and outer diameters 5.6 to 8.4 nm, low density and flexibility, make them good candidates for reinforcement in nanoscale fibre composite materials [9, 10]. The main aim in adding CNTs is to increase the tensile strength and elastic modulus of the composite [11]. However, dispersing CNTs in a metal matrix can be a challenging, due to the large difference in surface tension, which leads to poor wettability between the reinforcement and matrix alloy [12]. Ball milling has been shown to produce good dispersion of CNTs in metal matrix composites [11]. Mani. et al. [13] have found that even surface modification of CNTs by electroless plating

followed by ultrasonic agitation did not produce a uniform dispersion of reinforcement without ball milling.

Spark plasma sintering (SPS) is an advanced sintering method for the rapid consolidation of powders. Through the application of high pressures and electric currents, rapid heating rates (up to 1000 ˚C min^{-1}), and short sintering times (3-5 min), can be used to produce fully dense material [14]. This method has been explored in the fabrication of CNT-metal matrix composites, due to its ability to preserve nanoscale features [11, 15]. During SPS, the measured temperature is used to modulate the electric current in order to follow a set heating curve. However, temperature is measured using either thermocouples or pyrometers which are focussed on the punches and dies close to the sample, rather than on the sample itself. The temperature of the sample can therefore be significantly over or underestimated if large temperature gradients exist. More accurate ways to calibrate SPS temperature are therefore of great interest. Recently an accurate calibration of SPS temperature has been performed [16] using the phase transformation which occurs in soft magnetic FeCo alloy at the Curie point. The phase transformation alters the thermal and electrical conductivity of the alloy; leading to an anomalous pulse in the current-temperature curve. At this point the actual temperature of the sample (the Curie temperature) is known and can be compared with the corresponding thermocouple or pyrometer reading.

The objective of this study was to evaluate the effects of CNT addition on the mechanical and DC magnetic properties of Fe50Co composites prepared by SPS.

2. Experimental work

The binary gas atomised Fe50Co alloy powder was supplied by Sandvik Osprey Powder Group. A scanning electron microscope with energy dispersive X-ray spectrometer (EDS) attachment of oxford instrument was used to study the morphology and composition of the powders. A Malvern Mastersizer 3000 was used to measure the particles size distribution of the Fe50Co powder.

Multi-walled carbon nanotubes were provided by Haydale Ltd., which were functionalized using a plasma treatment to incorporate a covalently bonded oxide group to the surface. The key advantage of the functionalisation process is to improve the CNT dispersion in the solvent during colloidal processes by reducing the van-der-Waals forces between the nanotubes [17, 18]. Two different methods were used to mix iron cobalt alloy

powder with functionalised multi-walled carbon nanotubes. The first method (A) involved the dry mixing of the reinforcement with 20 g of binary Fe50Co alloy powder for volume fractions of 0.5 to 4.5 vol.%, followed by milling the mixture in a ball pestle impact grinder at BPR(1:1) for 1 h. The second method (B) involved the wet mixing of multi-walled carbon nanotubes with Fe50Co powder in dimethyformamide DMF for volume fractions of 0.5 to 3 vol. %. DMF is a commonly used solvent for dispersing carbon nanotubes [19]. The suspension of carbon nanotubes in DMF was stirred under ultrasonic agitation for 60 min. followed by the addition of 20 g of alloy to each suspension. The resulting slurry was sonicated for 30 min. The slurry was dried on a hot plate at the evaporation temperature for DMF (150˚C) overnight. The dried mixture was then milled in the ball pestle impact grinder at BPR (1:1) for 1 h.

The Fe50Co alloy and composite powder mixtures were consolidated in a graphite die using a spark plasma sintering furnace (HPD 25/1 FCT, Germany). All of the samples were heated to the sintering temperature at a constant rate of 50˚C/min under a vacuum of 1 hPa. An initial pressure of 7 MPa was applied from room temperature to 400˚C; followed by an increase to 80 MPa pressure and simultaneous heating to 900 °C for a 3 minute dwell [20]. Samples were left to cool in the furnace and extracted from the die using a manual hydraulic press. The Archimedes' immersion method in water was then used to measure the density of the compacts. The theoretical densities of the composites were calculated using the rule of mixtures. The theoretical densities for the CNT and FeCo powders were taken as 1.4 g cm^{-3} and 8.174 g cm^{-3} respectively for calculations.

Cross sections of the sintered materials were ground and polished with different grade abrasive discs followed by etching using 10% Nital for (30) sec. Optical microscopy and SEM were used to analyse the microstructural features. In order to evaluate the magnetic properties, samples with a rectangular cross section (24 mm × 5 mm) were cut from 30 mm diameter sintered disks using an electron discharge machining (EDM) cutting machine. Samples were ground using silicon carbide papers to remove the scratches from cutting. An automatic universal measurement system was used to evaluate the quasi DC magnetic response for samples by changing the magnetic field up to 25 kA/m [21]. Hardness measurements for both the matrix alloy and composites were performed at five different locations using a Vickers hardness tester with an applied load of 30 g for 4 sec. Tensile tests were performed on 3 samples cut from 30 mm diameter monolithic alloy and composites disks using EDM. The cut samples were ground using silicon carbide to remove any crack

initiation sites produced by the cutting. The tensile sample dimensions were (11 mm x 3 mm x 1.25 mm) [22]. The tensile mechanical properties of the materials were measured using a Shimadzu testing machine with a cross head speed of 2 mm/min.

3. Results and discussion

3.1. Characterisation of the starting powders and sintered materials

An SEM image of the Fe50Co alloy powder is shown in Fig. 1. Spherical particles with a wide size distribution are evident; Dv (10) 9.79 μm, Dv (50) 23.4 μm and Dv (90) 54.0 μm.

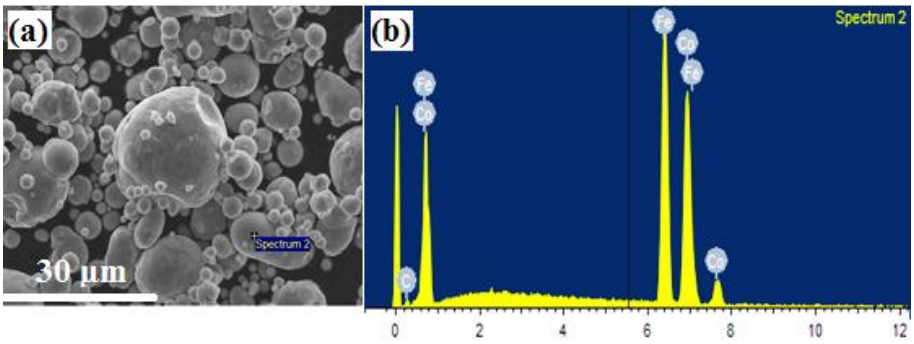

Fig.1. (a) SEM image and (b) EDS spectrum of as-received FeCo alloy powder.

TEM images of plasma treated CNTs are presented in (Fig.2), the arrows identify the defects which may be subdivided into dimensional and structural defects. Most of the CNTs are tangled with each other, which impedes their dispersion. The non-uniformity in the graphene layers, discontinuity on the inside of the fibres and defects on the outer surfaces suggest that the defects may not only be produced during fabrication but also by the functionalization processes. Amorphous carbon was observed on the surface of the fibres. These imperfections are preferred sites for chemical reaction. Some dark areas were observed on the CNTs which are probably metal inclusions, occurring from the reaction with the metallic catalyst used during their fabrication [17]. The measured dimensions of the CNTs exhibit a mean outer diameter of around 10.45 nm, while the inner diameter is around 4.29 nm. This corresponds to 34 concentric shells of carbon sheets in some cases, but for most CNTs, it was typically about 10. Caps were observed at the ends of some of the CNTs, while some tubes showed open ends. This opening of the hemispherical cap is due to oxidation during the functionalization step.

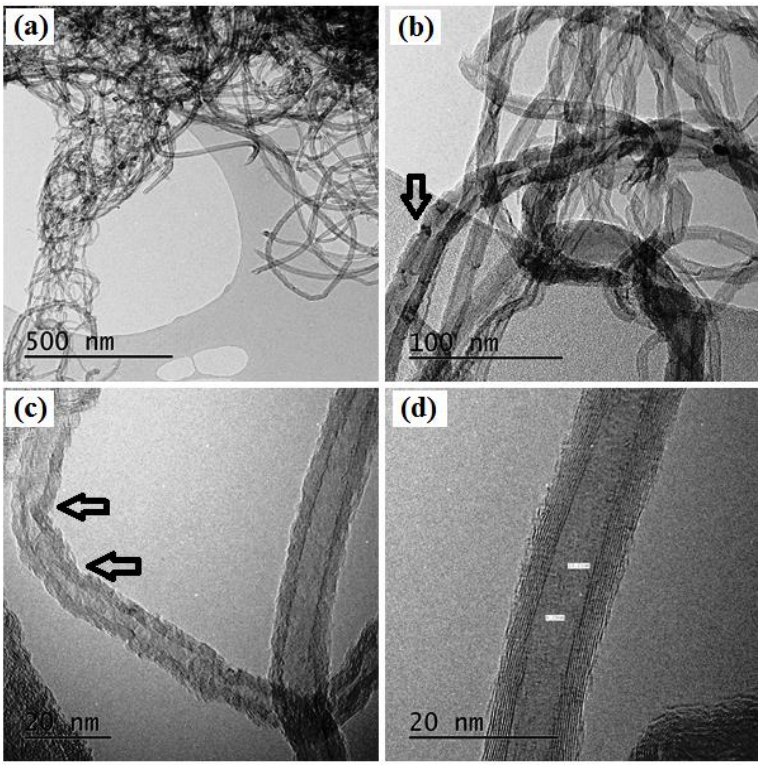

Fig.2. Transmission electron micrographs of plasma treated CNTs; the arrows highlight defects.

An XRD pattern of the as received CNTs, generated using a copper anode, is shown in Fig.3. The main peaks for carbon nanotubes were observed at 2θ values of ~26˚ and ~43˚ and are in good agreement with the pattern previously reported in [13]. The d_{002} calculated using the Bragg equation ($\lambda=2d\sin\theta$) is 0.3445 nm which is consistent with spacing for graphite of 0.3348 - 0.3360 nm (5% experimental error). A broadening of the peak at ~26˚ could be observed, and is likely due to the presence of oxides introduced to the CNTs during functionalization process; with the variation in d spacing due to the incorporation of oxygen between the lattice planes. Broadening could also be due to contributions from the amorphous regions of the CNTs.

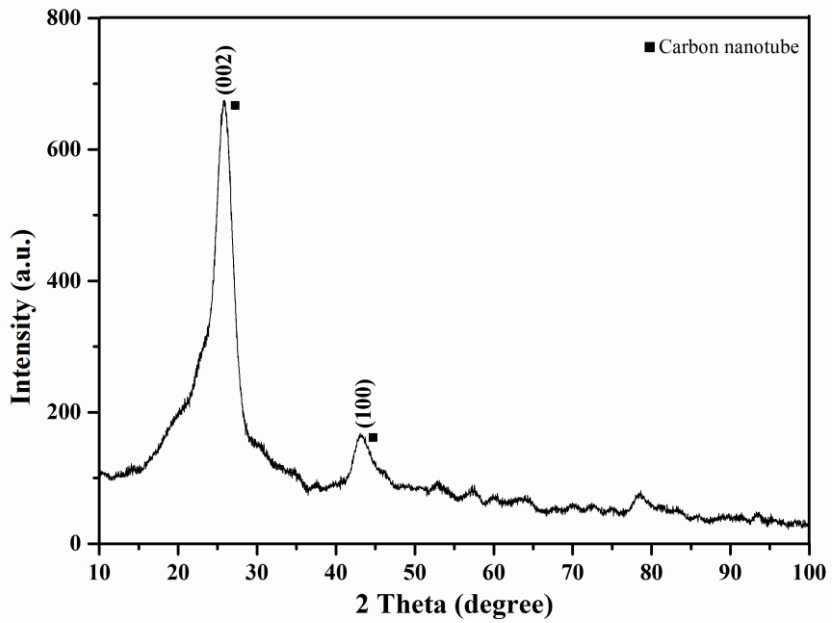

Fig.3. XRD pattern of as received CNTs, the main diffraction planes are labelled.

The densification behaviour of as received monolithic FeCo alloy and composite were different as shown in Fig.4. The volume fraction of reinforcement affected the densification behaviour. The composite materials densified at lower temperatures compared to as received alloy, which could be due to the influence of CNTs on the densification mechanism. In addition the ball milling step decreased the particle size in the composite which increased the surface area between reactants; leading to faster densification kinetics through improved mass transport by diffusion [23, 24]. The densities of the composites containing up to 1.5 vol.% CNT were higher as compared to the monolithic Fe50Co alloy Fig.5. The highest density was achieved for the 0.5 vol. % CNTs composites; while the density dropped sharply at higher volume fractions. This is due to the increased agglomeration of the CNTs, which induces porosity in the composite material.

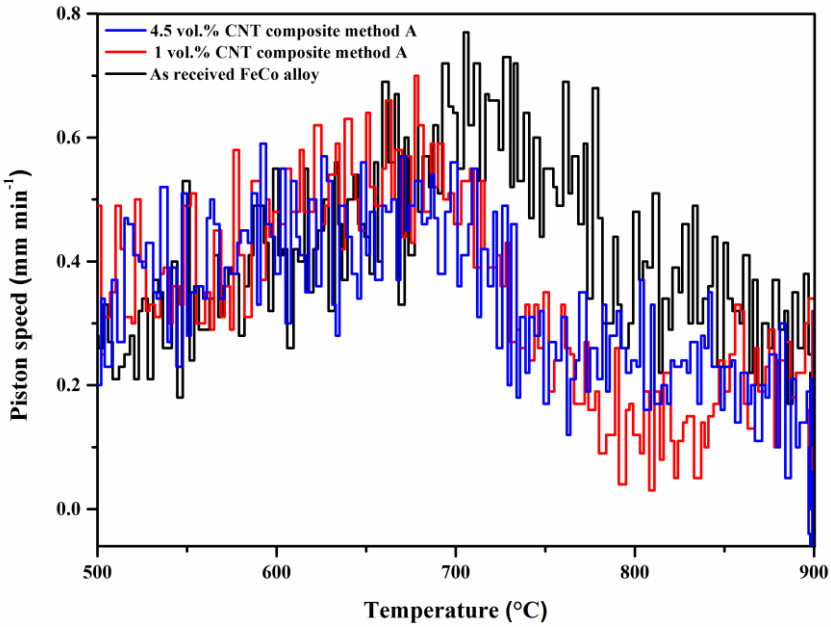

Fig.4. Shrinkage sintering curve, for the as received FeCo alloy in comparison to the 1 and 4.5 vol.% CNT composite materials prepared using method A.

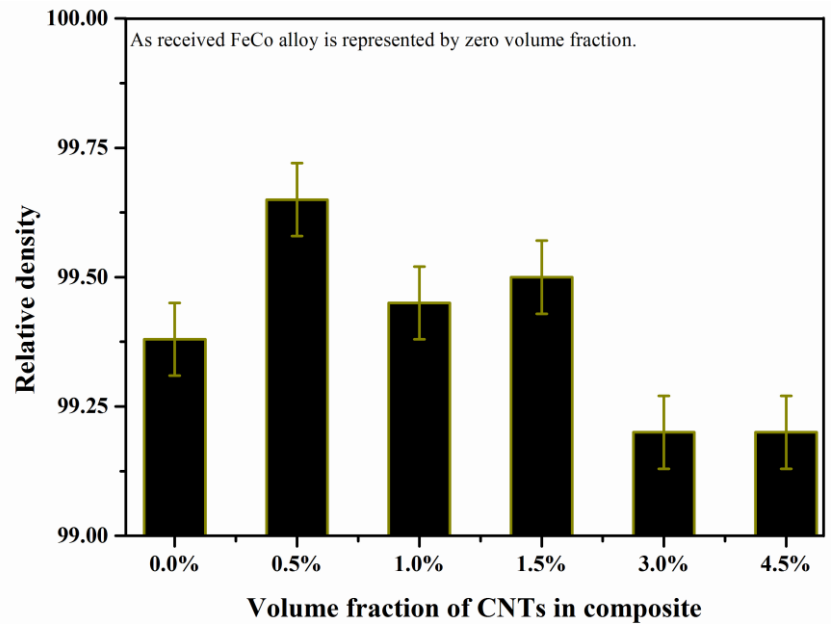

Fig.5. Variation of relative density of SPS sintered composite materials fabricated using method A against volume fraction of CNTs (%) compared to monolithic FeCo alloy.

Fig.6 shows a comparison between monolithic FeCo alloy powders before and after ball milling processes. The peaks after 1.5 h ball in air atmosphere are identical to the maghemite phase. The powder is heated up during ball milling, leading to formation oxide layer which deteriorates densification during sintering because it forms a diffusion barrier during sintering.

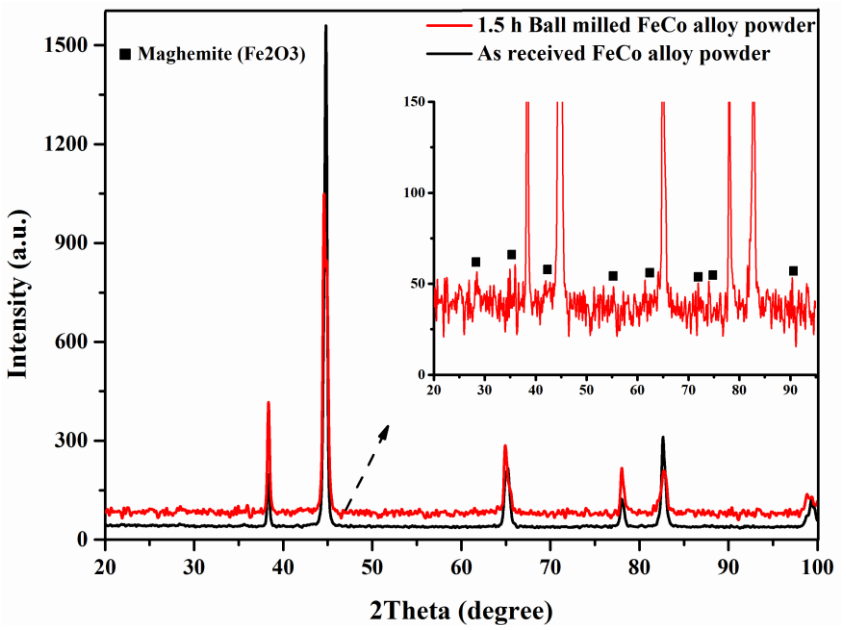

Fig.6. XRD shows oxidation of FeCo alloy due to ball milling in air atmosphere.

Fig.7 (a and b) show slow scan XRD patterns (Co Kα) for the sintered Fe50Co as received, ball milled and composite forms. The enlarged pattern of the (100) peak (Fig.7 b) was used to observe the ordering of the Fe50Co alloy, which was scanned in the range of the expected superlattice line [4]. The pattern shows that the addition of 1 vol. % CNTs with ball milling produced a reduction in the antiphase domain size for the ordered crystalline phase. The crystallite domain sizes were calculated using the Scherrer equation of the (100) peak (Fig.7 b) as 45.75 nm to 28.10 nm and 34.32 nm for as received Fe50Co alloy, 1 vol. % CNT and 4.5 vol. % CNT, respectively. The composite with a higher volume fraction of CNTs displayed an increase in crystallite size, yet a high intensity of ordering was observed in the XRD patterns. As such, it appears that an increase in the volume fraction of CNTs produces an increase in the volume fraction of ordering as compare to the monolithic alloy and low volume fraction composites. Strains are classified to uniform strain and nonuniform strain, the former shifting peaks of x-ray reflection to lower angles, while the latter lead to broadening and reduce the intensity [25]. Ball milling processes can induce stresses in powder, however the intensity of ball milling was very low as the process was performed for BPR 1:1 for 1 h to disperse the reinforcement in the base alloy. Residual stress may be released during sintering at high temperature. This suggests the effects of strain on broadening x-ray reflection are minimal, as the recovery reduces the magnitude of the residual stress and recrystallization completely eliminates the residual stress leading to the maximum sharpness in diffraction line [25].

(a)

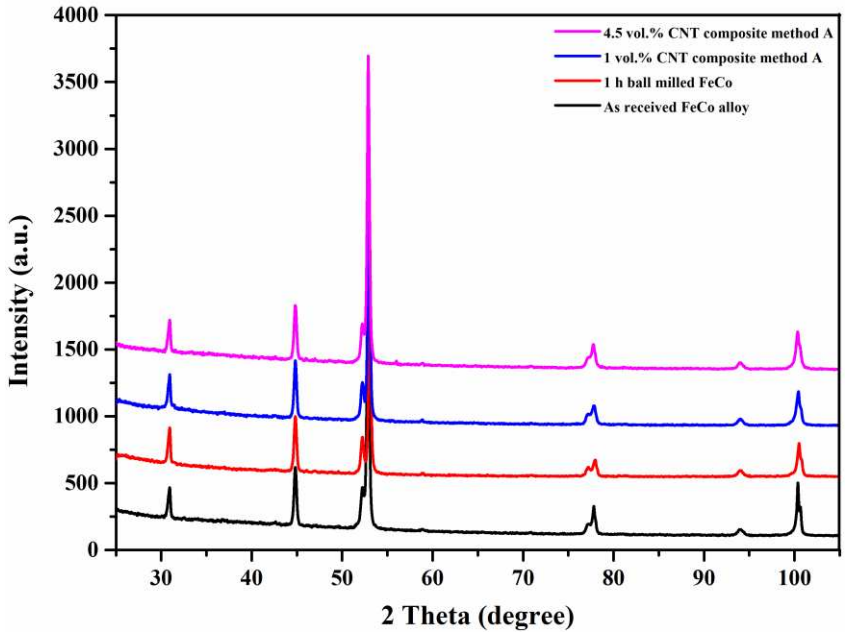

(b)

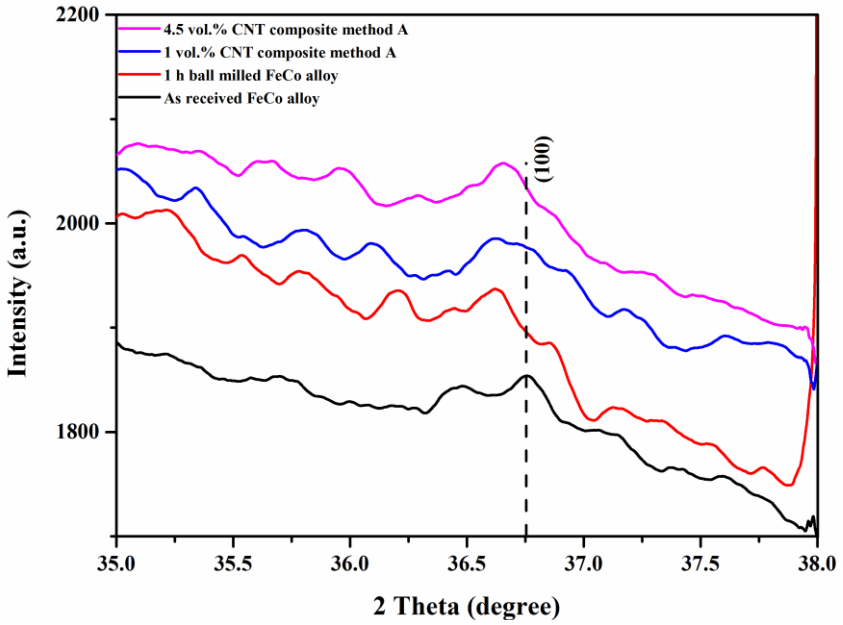

Fig.7. XRD patterns (a) slow scan for sintered FeCo as received alloy, 1 h ball milled FeCo alloy, 1 vol.% CNT composite and 4.5 vol.% CNT composite; (b) (100) Superlattice peak for displayed material.

The optical micrographs for both the Fe50Co alloy and the composites are shown in Fig.8. A very fine microstructure was observed for the 0.5 vol. % CNT composite, which reflects the role of CNTs in refining the microstructure. However, this behaviour is different at higher volume fractions of CNTs due to the segregation of carbon nanotubes to the grain boundaries; which cause an increase in the thickness of the grain boundaries of the composite materials compared to the monolithic alloy. This agglomeration causes poor densification at

higher volume fractions. Pores and elongated grains were observed at high volume fractions. The ball milling process changes the shape of the powder particles; and as a result, an elongated grain structure is observed after sintering. This structure becomes more evident due to the increasing fraction of agglomeration and the poor densification at high volume fraction of CNT. No difference can be observed in the microstructure between the two methods used to prepare the composites.

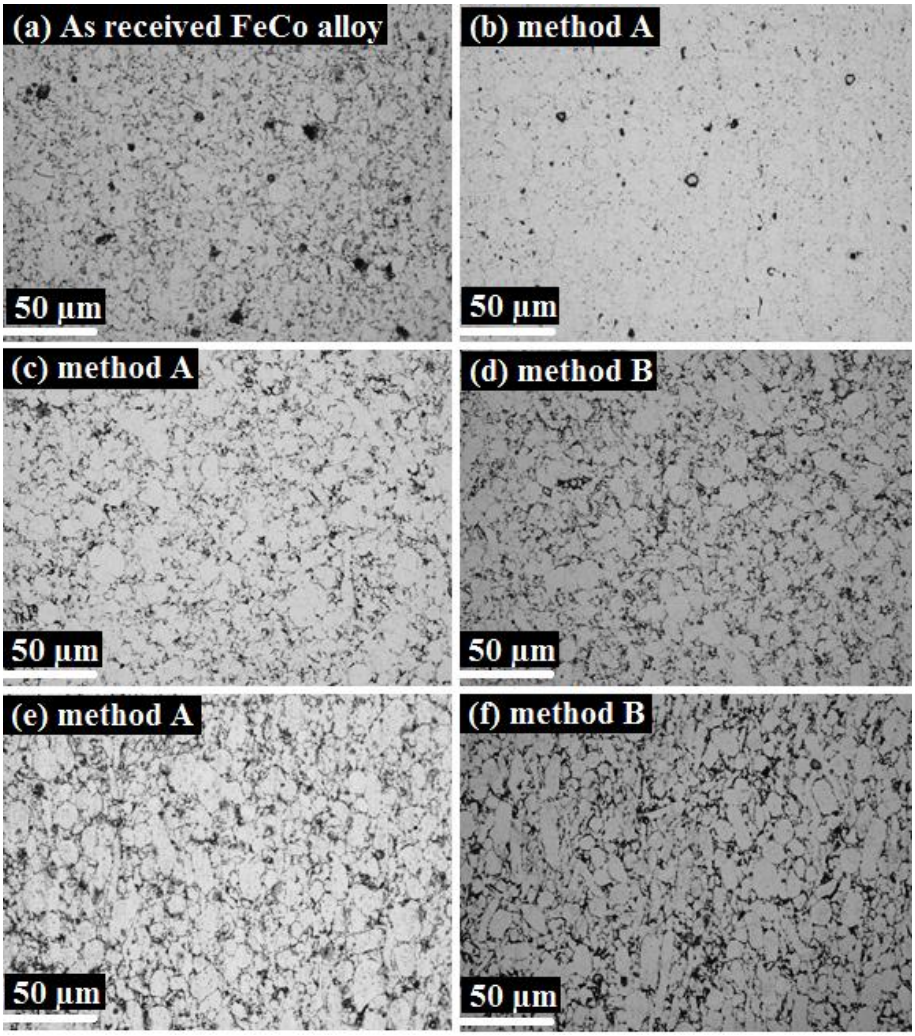

Fig.8. Optical microstructure of: (a) FeCo alloy; images (b), (c) and (e) are 0.5 vol.%, 1 vol.% and 3 vol.% CNT composite, respectively prepared by method A. Images (d) and (f) are 1 vol.% and 3 vol.% CNT composite, respectively prepared by method B.

3.2. Magnetic and mechanical properties

The magnetic properties of the Fe50Co alloy and composite materials fabricated following mixing methods A and B are summarised in Fig.9.

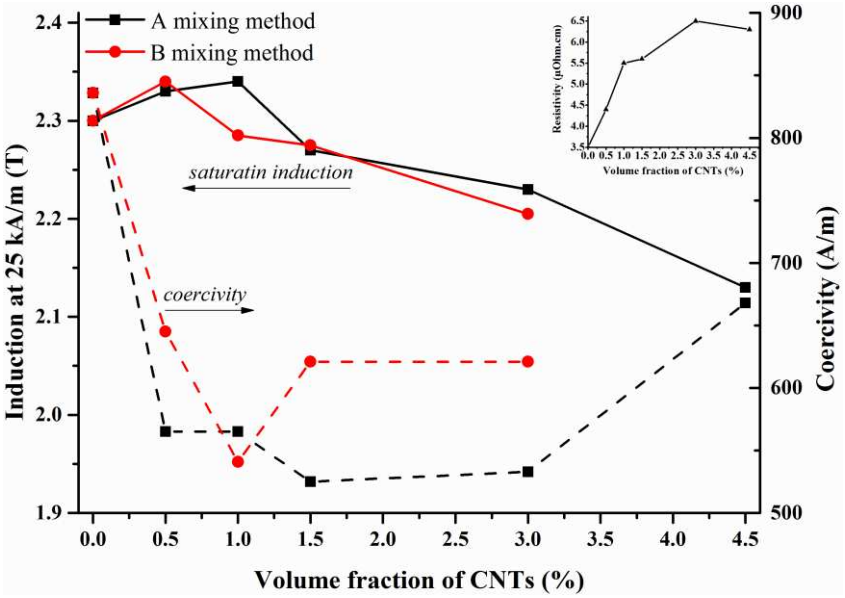

Fig.9. Effect of volume fraction of CNTs on: saturation induction; coercivity of (Fe50Co)-CNT composites fabricated by two different dispersion method followed by spark plasma sintering. The monolithic alloy is represented as 0 vol.% CNT. The insert curve shows the change in resistivity with increasing volume fraction of CNTs for composites prepared using method A.

It is clear that the saturation induction is highly dependent on sample density; with the saturation induction trend closely following that of the density trend (Fig.5) with increasing volume fraction of CNTs. The highest saturation induction was achieved in the composite material at 1 vol. % CNTs, consistent with it having a high density. With an increased volume fraction of CNTs, a drop in saturation is seen due to the agglomeration of the reinforcement as observed in (Fig.8) and the subsequent of that drops in density.

A drop in coercivity was observed in the composites produced by both fabrication methods in comparison to the monolithic Fe50Co alloy. Coercivity is typically inversely proportional to the grain size; however, the results indicate a decrease in coercivity with decreasing grain size. Previous models in [26, 27] have explained this behaviour in terms of the anisotropy energy. For a very small grain size (D) < 100 nm the ferromagnetic exchange length will often be larger than the grain size (D). The exchange length in a soft magnetic alloy is calculated by using the following equation:

$$L_{ex} = (A/K_1)^{-1/2} \quad \text{(Equation1)}$$

Following eq.1 and using exchange constant $A=1.7\times10^{-11}$ J/m and magnetic anisotropic constant $K_1=8$ kJ/m^3 for calculation the exchange length in Fe50Co alloy [28], giving $L_{ex}=46$

nm, which is in value higher than the measured ordered crystallite size, meanwhile the change in coercivity with crystallite size follows Néel's model. As a consequence, the effective anisotropy energy is averaged over a number of grains and is thus reduced in magnitude. In this anomalous behaviour of nanocrystalline magnetic materials, the coercivity exhibits D^6 dependence, which is in contrast to the conventional rule for polycrystalline magnetic materials, which exhibit 1/D dependence. As discussed previously, the Scherrer calculations show a crystallite size below 100 nm in the monolithic Fe50Co, which decreases further for the composite samples. This may therefore account for some of the trends seen in coercivity. However, at the highest volume fraction of CNTs the coercivity increased. Néel [29] suggested that the coercivity is directly proportional to the volume fraction of non-magnetic inclusions. Residual stresses produced due to the difference in the coefficient of thermal expansion between the CNTs and the monolithic Fe50Co alloy may lead to domain wall pinning, thereby increasing coercivity and creating a trade-off between coercivity decrease due to grain size and increase due to domain wall pinning as the volume fraction of reinforcement is increased.

A high resistivity is crucial for producing low loss components. Resistivity measurements of the monolithic Fe50Co alloy and CNT composites fabricated using method A are shown as an insert in Fig.9. A slight increase in resistivity is observed from 3.5 μΩ.cm for monolithic Fe50Co alloy to 5.6 μΩ.cm for the composite with the highest density up to 1.5 vol. % CNTs. Higher volume fractions of CNTs (3 and 4.5 vol. %) further increase the resistivity of composite materials, which may be due to the increase in the level of porosity.

The tensile strength and the mechanical hardness of the Fe50Co alloy and composite materials prepared using the two different methods are summarized in Fig.10 and Fig.11 respectively. The addition of a small amount of CNTs up to 1vol. % produces an improvement in tensile strength in comparison to the base alloy. The greatest improvement is observed with the addition of 0.5 vol. % CNTs. In this case a tensile strength and Vickers hardness of 821 ±30.77 MPa and 352 ±15.15 VHN, respectively were measured. The mechanisms for an improvement in the mechanical properties of composite materials include load transfer between the matrix and reinforcement, grain size refinement and dislocation strengthening mechanisms. The mechanical properties are highly correlated to the grain size of Fe50Co alloys; following the Hall-Petch relationship in both the ordered and the disordered state [30].

$\sigma_y = \sigma_i + k_y d^{-1/2}$ …… (Equation 2)

where σ_y is the yield strength, d is the average grain diameter, σ_i is a materials constant describing the intrinsic resistance of the lattice to dislocation motion, and k_y is the strengthening coefficient.

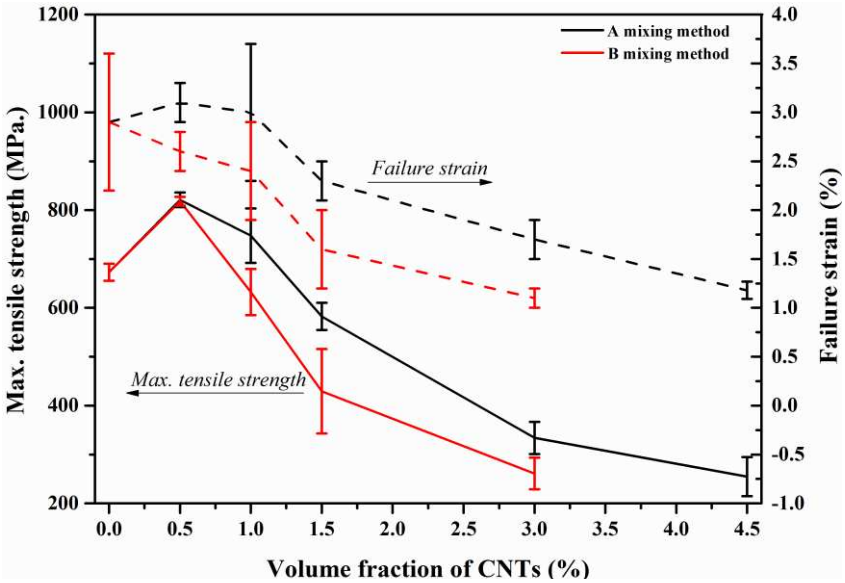

Fig.10. Effect of volume fraction of CNTs on: tensile strength (solid lines) and failure strain (dashed lines) of (Fe50Co)-CNT composites fabricated by two different dispersion methods followed by spark plasma sintering; the monolithic alloy is represented as 0 vol.% CNT.

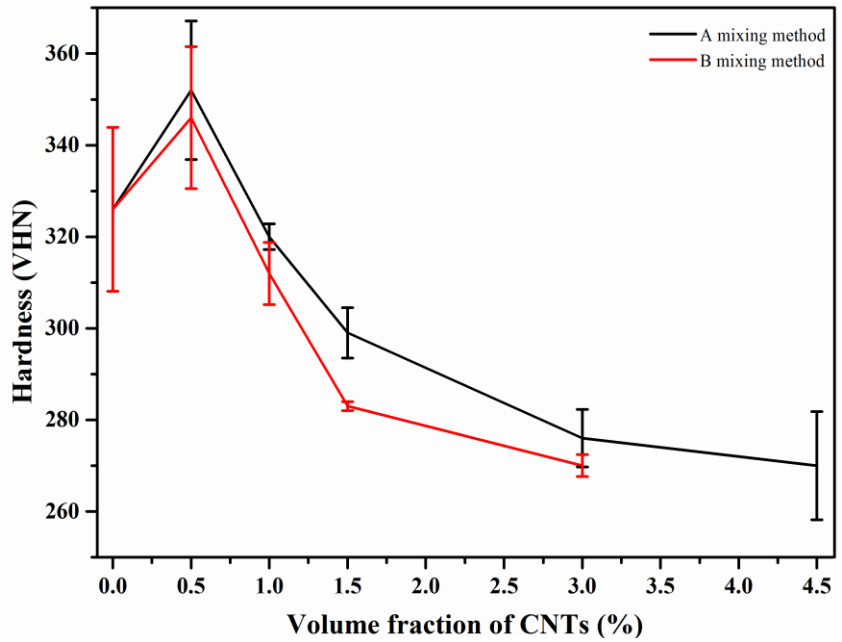

Fig.11. Effect of volume fraction of CNTs on: hardness of (Fe50Co)-CNT composites fabricated by two different dispersion methods followed by spark plasma sintering; the monolithic alloy is represented as 0 vol.% CNT.

The optical micrographs of the Fe50Co composites show that the addition of a low volume fraction 0.5 vol. % of CNTs refines the microstructure and improves densification. As a result, an increase in tensile strength and hardness at low volume fractions is achieved. However, the mechanical properties deteriorate at higher volume fractions of reinforcement using both fabrication processes. The decrease was higher for composites produced using mixing method B. It was experimentally observed that the CNTs tended to separate as a surface layer on the powder after drying using method B, leading to more agglomeration of the CNTs and subsequently poorer densification.

An increase in the failure strain was observed in the composites containing low volume fractions of reinforcement. EDS results for monolithic Fe50Co alloy and its composites show a deviation in the chemical composition of the composite in comparison to the monolithic Fe50Co alloy. This suggests that the CNTs lead to chemical deviations in the matrix surrounding them. It has been reported [6] that particles in Fe50Co alloy cause a chemical deviation in the matrix around them, which could lead to disorder around the inclusions and possible improvement in the ductility. Moreover, additions of small amounts of CNTs lead to the development of a very fine microstructure, and may form metal carbides as a result of the reaction with any amorphous carbon on the CNTs. This may not necessarily be detectable by XRD since the amount of carbides produced would be lower than the sensitivity of the technique. These two parameters play an important role in the improvement of ductility, as has been reported previously [31].

Fractographic images of the monolithic alloy and composite materials with different volume fractions of CNTs are shown in Fig.12. Mixed modes of fracture between intergranular and transgranular were observed for both the monolithic alloy and the composite materials. Small tubular holes were observed in the fracture surface, as indicated by arrows in image (c), which are likely to be the former locations of CNTs which were extracted during fracture. Porosity can be seen to increase at high volume fractions of CNTs, as shown in image (d), while images (e) and (f) show the agglomeration of CNTs between powder particles. The high magnification insert in (f) shows the presence of CNT bundles at the boundary. These bundles would have hampered densification in the composite.

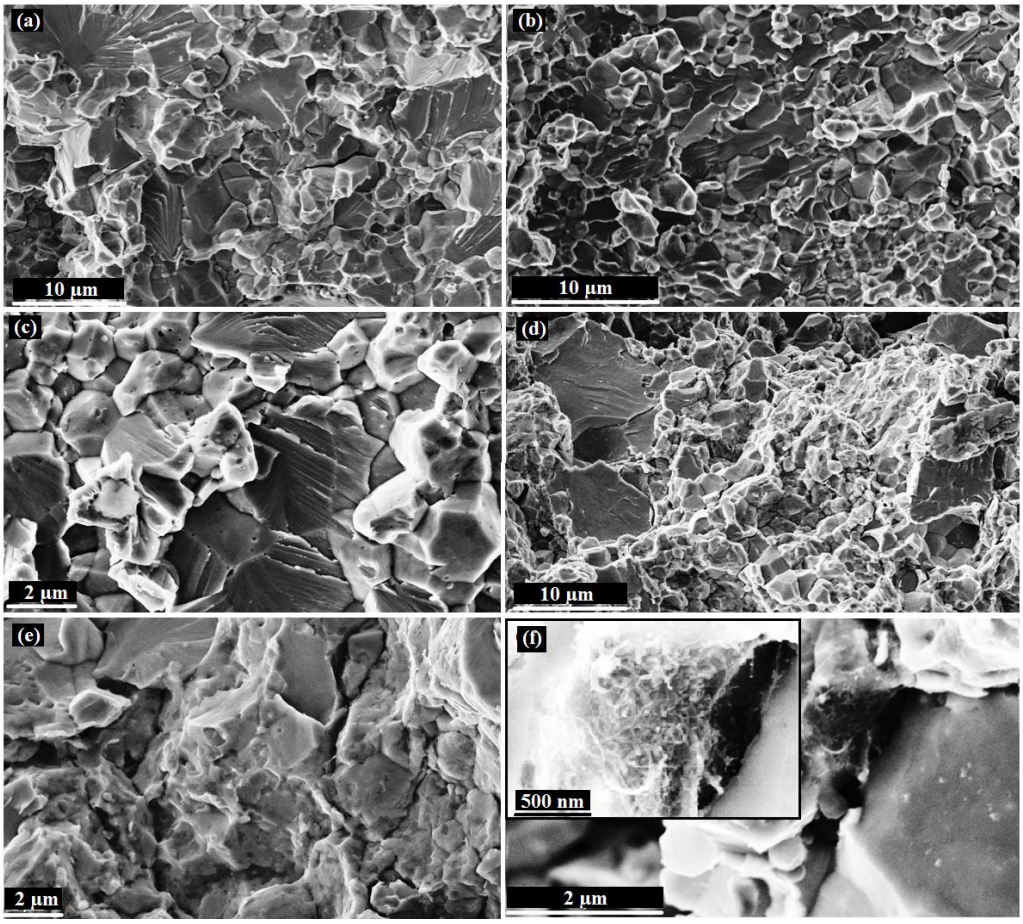

Fig.12. Fractographic images of materials prepared using processing rout A : (a) FeCo monolithic alloy; (b) 0.5 vol.% CNT composite; (c) 1 vol.% CNT composite; (d) 1.5 vol.% CNT composite; (e) 3 vol.% CNT composite; (f) 4.5 vol.% CNT composite. High magnification image insert in (f) shows CNTs bundle between powder particles boundaries.

3.3. Raman spectroscopy

Raman spectroscopy is a non-destructive test, which is a powerful tool largely used for the characterisation of various carbon based materials for determining the degree of structural ordering or presence of contaminants. The characteristic bands in all the graphite based materials, including MWCNT, can be classified into: first-order and second-order Raman spectra [32]. The former shows a tangential stretching G mode at (1500-1600 cm^{-1}), in addition to the D mode around 1350 cm^{-1}. There is also an exceptional band, which can only be observed in SWNT, and is a radial breathing mode (RBM) in the range 100 cm^{-1} to 400 cm^{-1} [32, 33]. Furthermore a weak shoulder band (D') is observed around 1620 cm^{-1}on the right side of the G band. The second order spectra are characterised by the main peaks of (G') at 2705 cm^{-1} and (D+G) at 2945 cm^{-1} [32]. The relative intensities between the D band,

which is related to structural defects, and G band, which is related to the order of the graphite structure ($R=I_D/I_G$) is widely used to evaluate the defect density of carbon nanomaterials and carbonous nanocomposite [34, 35]. Fig.13 (a and b) show the Raman results for the (Fe50Co)-CNT composites and the change in R ratio for the raw plasma treated MWCNTs and the composites fabricated by the two different methods with respect to the volume fraction of CNTs.

A split in the G band was observed, which demonstrates that the integrity of CNTs is maintained throughout the fabrication process, as reported in [23]. The main reason for this is due to the stronger tube morphology of the CNTs in contrast to the flat morphology of graphene sheets. However, the splitting in the G band is less pronounced in MWCNT and in large radius CNTs. This suggests that a thinning in the radius of the CNTs may occur during the fabrication process, reducing the number of layers; or that the radii of the majority of the CNTs in the powder are in the range of band splitting, since DWCNTs were observed in TEM images. Mixing method B gives a high value of R at low volume fraction, which reflects the effect of the processing route on the quality of CNTs. The damage of the CNTs was reduced at higher volume fraction as compared to mixing method A. This could be due to a the less effective ultrasonic dispersion processing of higher volume fractions of CNTs, due to a less effective transmission of the ultrasonic wave in solution, leading to a greater segregation of CNTs on the surface of the slurry. With dispersed 'pockets' of CNTs present in the powder, many of the CNTs were therefore shielded from damage during ball milling. Inam et al. [36] reported that the structural features of the CNTs in composites are very sensitive to the spark plasma sintering conditions and to the matrix material. This means that the improvement in the quality of CNTs could be due to the effective thermal annealing during cooling in SPS furnace following the sintering process. The stress on the surface of the CNTs introduced by the functionalization process may be released by removing defects and oxides from the CNTs. Improvement in quality of carbon nanostructure composite consolidated by SPS has been observed in [37].

(a)

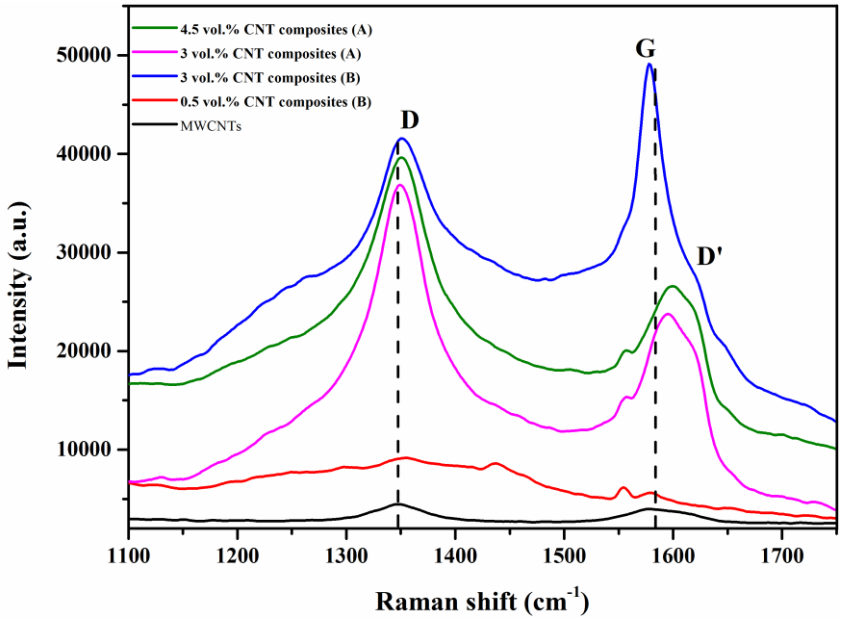

(b)

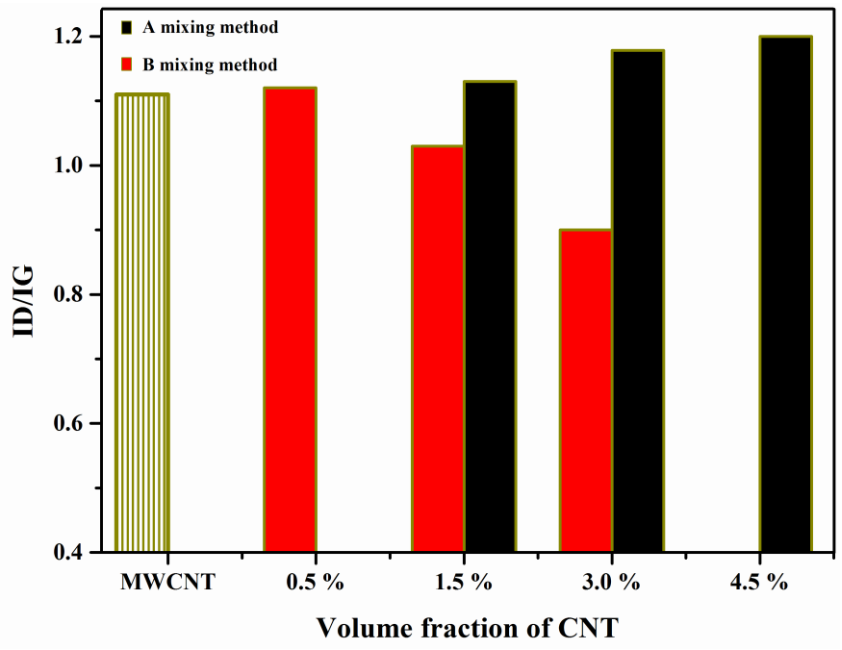

Fig.13. (a) Raman spectra of MWCNTs and FeCo alloy composites; (b) Intensity ratio($R = I_D/I_G$) of composite fabricated by the two methods.

4. Conclusions

1-The addition of CNTs improved the mechanical properties of the binary Fe50Co alloy; with 0.5 vol. % of carbon nanotubes giving the maximum increase in tensile strength of around 20 %. Low volume fraction composites had a higher failure strain (3.1 %).

2-The magnetic properties were improved by the addition CNTs up to 1 vol. %, while a sharp deterioration in properties were occurred at high volume fractions as a result of poor dispersion and densification.

3-Dispersing CNTs using ball milling improved the densification of the composite material as compared to the as received binary Fe50Co alloy. This was due to the reduced grain size produced from ball milling and CNT addition, especially at low volume fraction. Here further inhibition of grain growth was provided by the CNTs during spark plasma sintering. A cleaning of the grain boundaries also occurred during SPS, leading to an improvement in density in the monolithic Fe50Co alloy.

4-The ball milling of an unmixed powder in a solvent produced a superior CNT dispersion, as compared to ball milling following wet mixing in DMF under ultra-sonication. Ultra-sonication produced an increase in ($R=I_D/I_G$) for composites with a low volume fraction of CNTs. However a decrease was seen at higher volume fraction due to the agglomeration of the powder, which prevented direct contact between the milling balls and the CNTs.

References

[1] R. S. Sundar, and S. C. Deevi: Soft magnetic FeCo alloys: alloy development, processing, and properties. International Materials Reviews 50, 3 (2005).

[2] D. W. Clegg, and R. A. Buckely: The Disorder- order transformation in Iron-Cobalt based alloys. Metal Science 7, (1973).

[3] R. H. Yu, S. Basu, L. Ren, , Y. Zhang, , A. Parvizi-Majidi, , K.M., Unruh, and J. Q. Xiao: High Temperature Soft Magnetic Materials:FeCo Alloys and Composites. IEEE Transactions on Magnetics. 36, 5 (2000).

[4] E.P George, A. N. Gubbi, I. Baker, and L. Robertson: Mechanical properties of soft magnetic FeCo alloys. Materials Science and Engineering A329, 331(2002).

[5] L. Zhao, and I. Baker: The effect of grain size and FeCo ratio on the room temperature yielding of FeCo. Acta metall. mater. 42, 6 (1994).

[6] L. Zhao, I. Baker, and E.P. George: Room temperature fracture of FeCo. Proceedings of the Materials Research Society 288, (1993).

[7] P. Bowen, and T.J.A. Doe: Tensile properties of particulate-reinforced metal matrix composites. Composites. A 27A, (1996).

[8] M. Kumar, G. Viola, M.J. Reece, J. Hall, and S. Evans: Influence of coated SiC particulates on the mechanical and magnetic behaviour of Fe–Co alloy composites. J. Materials Science. 49, 6 (2013).

[9] M.M.J. Treacy, T.W. Ebbesen, and J.M. Gibson: Exceptionally high Young's modulus observed for individual carbon nanotubes. Nature. 381, (1996).

[10] X. Chen, J. Xia, J. Peng, W. Li, and S. Xie: Carbon-nanotube metal-matrix composites prepared by electroless plating. Composite Science and Technology. 60, (2000).

[11] S. R. Bakshi, D. Lahiri, and A. Agarwal: Carbon nanotube reinforced metal matrix composites-a review. International Materials Reviews. 55,1(2010).

[12] F.Z. Kong, X.B. Zhang, W.Q. Xiong, , F. Liu, W.Z. Huang, Y.L. Sun, J.P. Tu, and X.W. Chen: Continuous Ni-layer on multiwall carbon nanotubes by an electroless. Surface and Coatings Technology. 155, (2002).

[13] M. Mani, G. Viola., M. Reece, , S. L. Evance. and J. Hall: Improvement of interfacial bonding in carbon nanotube reinforced Fe–50Co composites by Ni–P coating: Effect on magnetic and mechanical properties. Materials Science and Engineering B 188, (2014).

[14] X. Song, X. Liu, and J. Zhang: Neck Formation and Self-Adjusting Mechanism of Neck Growth of Conducting Powders in Spark Plasma Sintering. Journal of the American Ceramic Society. 89, 2 (2006).

[15] N. Saheb, Z. Iqbal, A. Khalil, A. Hakeem, N. Al Aqeeli, T. Laoui, A. Al-Qutub, and R. Kirchner: Spark Plasma Sintering of Metals and Metal Matrix Nanocomposites: A Review. Journal of Nanomaterials. 2012, (2012).

[16] M. Kumar, G. Viola, J. Hall, S. Grasso, and M. Reece: Observations of Curie point transition during Spark Plasma Sintering of ferromagnetic materials. J. Mag. and Mag. Mat. 382, (2015).

[17] A. Hirsch, and O. Vostrowsky: Functionalization of Carbon Nanotubes. Springer Berlin Heidelberg 245, (2005), pp. 193, 237.

[18] J.L. Bahr, J. Yang, D.V. Kosynkin, M.J. Bronikowski, R.E. Smalley, and J.M. Tour: Functionalization of carbon nanotubes by electrochemical reduction of aryl diazonium Salts: a bucky paper electrode. Journal of the American Chemical Society. 123, 27 (2001).

[19] H. Ham, Y. Choi, I. Chung: An explanation of dispersion states of single-walled carbon nanotubes in solvents and aqueous surfactant solutions using solubility parameters. Journal of Colloid and Interface Science. 286, 1 (2005).

[20] M. Mani, G. Viola., M. Reece, J. Hall, S. Evans: Structural and magnetic characterization of spark plasma sintered Fe-50Co alloys. Materials Research Society. 1516, (2012).

[21] P. Anderson: A universal DC characterisation system for hard and soft magnetic materials. Journal of Magnetism and Magnetic Materials. 320, 20 (2008).

[22] E. D. George: Mechanical Metallurgy, 3th ed. (McGraw-Hill, 1986), pp.295.

[23] A.M. Locci, R.Orru, G. Cao, and Z.A Munir: Effect of ball milling on simultaneous spark plasma synthesis and densification of TiC–TiB2 composites. Materials Science and Engineering A. 434, (2006).

[24] K.E. Thomson, D. Jiang, R.O. Ritchie, and A.K. Mukherjee: A preservation study of CNTs in alumina-based nanocomposites via Raman spectroscopy and nuclear magnetic resonance. Appl. Phys. A89, (2007).

[25] B.D. Cullity: Elements of X-ray diffraction, 2end ed. (Addison-Wesley publishing company, United States of America, 1978), pp 284,288.

[26] R. Alben, J.J. Becker, and M.C Chi: Random anisotropy in amorphous ferromagnets. Journal of Applied Physics. 49, (1978).

[27] G. Herzer: Grain size dependence of coercivity and permeability in nanocrystlline ferromagnets. IEEE Transactions on Magnetics. 26, 5 (1990).

[28] G. Couderchon, and J.F. Tiers: Some aspects of magnetic properties of Ni-Fe and Co-Fe alloys. Journal of Magnetism and Magnetic Materials. 26, 1(1982).

[29] F. Pfeifer, and C. Radeloff: Soft magnetic Ni-Fe and Co-Fe alloys- some physical and metallurgical aspects. Journal of Magnetism and Magnetic Materials. 19,1-3 (1980).

[30] A. Duckham, D.Z. Zhang, D. Liang, V. Luzin, R.C. Cammarata, R.L. Leheny, C.L. Chien, T.P. Weihs: Temperature dependent mechanical properties of ultra-fine grained FeCo–2V. Acta Materialia. 51, 14 (2003).
[31] K. Kawahara: Effect of carbon on mechanical properties in Fe50Co50 alloy. Journal of Materials Science. 18, (1983).

[32] E.F. Antunes, A.O. Lobo, E.J. Corat, V.J. Trava-Airoldi, A.A. Martin, C. Verı´ssimo: Comparative study of first- and second-order Raman spectra of MWCNT at visible and infrared laser excitation. Carbon. 44, 11 (2006).
[33] S. Osswald, , M. Havel, and Y. Gogotsi: Monitoring oxidation of multiwalled carbon nanotubes by Raman spectroscopy. Journal of Raman Spectroscopy. 38, 6 (2007).
[34] R. Saito, M. Hofmann, G. Dresselhaus, A. Jorio, and M. S. Dresselhaus: Raman spectroscopy of graphene and carbon nanotubes. Advances in Physics. 60, 3 (2011).
[35] H. Kwon, M. Estili, K. Takagi, T. Miyazaki, A. Kawasaki: Combination of hot extrusion and spark plasma sintering for producing carbon nanotube reinforced aluminum matrix composites. Carbon. 47, 3 (2009).

[36] F. Inam, H. Yan, M. Reece, T. Peijs: Structural and chemical stability of multiwall carbon nanotubes in sintered ceramic nanocomposite. Advances in Applied Ceramics. 109, 4 (2010).

[37] A.J. Albaaji, E.G. Castle, M.J. Reece, J.P. Hall, and S.L. Evans: Synthesis and properties of graphene and graphene/carbon nanotube-reinforced soft magnetic FeCo alloy composites by spark plasma sintering. Journal of Materials Science. 51, 16 (2016).